Article

An Investigation into the Metabolic Differences between Conventional and High Seeding Density Fed-Batch Cell Cultures by Applying a Segmented Modeling Approach

Teresa Laura Krumm [1],*[ID], Alireza Ehsani [2], Jochen Schaub [1] and Fabian Stiefel [1]

[1] Boehringer Ingelheim Pharma GmbH & Co.KG, Development Biologicals Germany, Birkendorfer Strasse 65, D-88397 Biberach an der Riß, Germany
[2] Boehringer Ingelheim Pharma GmbH & Co.KG, Biopharmaceuticals Germany, Birkendorfer Strasse 65, D-88397 Biberach an der Riß, Germany
* Correspondence: teresa.krumm@boehringer-ingelheim.com

Abstract: The conventional fed-batch process characterized by a low titer currently challenges pharmaceutical development. Process optimization by applying a perfusion process in the pre-stage and subsequent production phase at a high seeding density (HSD) can meet this challenge. In this study, we employed a simplified approach based on measured experiments, namely segmented modeling, to systematically analyze an HSD fed-batch process compared to a standard process. A comparison indicated that the metabolic phases of HSD processes are not only shifted in time, but metabolite trends show an altered metabolism. In an extended study, we integrated the intracellular fluxes determined by a metabolic flux analysis into the segmented modeling approach. Compared to using only extracellular rates, similar phases are identified, and this highlights the reliability of phase identification modeling using extracellular rates only. Furthermore, the segmented linear regression approach is used to create a model that describes cellular behavior and that can be used to predict potential improvements in the feeding strategy and in harvest viability. Here, overfeeding was eliminated and a significantly higher titer was achieved. This work provides insights into the overall metabolic changes in the HSD process and paves the way towards the optimization of the feeding regime.

Keywords: intensified fed-batch; segmented modeling; feeding optimization

1. Introduction

The biopharmaceuticals market focusing on monoclonal antibodies (mAbs) has been growing rapidly in recent decades [1]. Chinese hamster ovary (CHO) cells are the preferred cells for the production of monoclonal antibodies [2]. The conventional process starts with a seed train in several batch passages to generate enough cells to inoculate the final production process, which is performed in fed-batch mode. One characteristic of the fed-batch process is the continuous or periodic addition of a concentrated feed medium to replenish nutrients [3]. The conventional standard (STD) fed-batch production process is characterized by two phases: the growth phase and the stationary phase. Most of the product is generated in the stationary phase.

Future manufacturing capacities will be challenged by a high number of molecules in the pipeline, especially in the case of multi-specific antibody formats that are difficult to express [4,5]. Therefore, there is a need to increase the titer of the conventional fed-batch processes and to achieve a higher productivity. This will also lead to an improved facility utilization via product optimization [6]. To achieve a higher titer, the accumulation of cell mass in the growth phase in the production stage is shifted into the N-1 expansion stage. This shift occurs via perfusion and subsequent application of high seeding cell densities

in N-stage production [7]. This process type is called the high seeding density (HSD) fed-batch process.

Optimization of the cell culture process requires an in-depth knowledge of the cell behavior. Mathematical modeling can provide a deep understanding of the mechanisms and complex interactions in the cell culture process. The current popular methods of mechanistic and stochastic modeling often use complex models and depend on specific model analysis tools [5–8]. In this work, we employ a simplified approach to identify metabolic phases and to study the rationale behind the cell responses to environmental changes in the cell culture process in different process settings. We systematically analyzed two different process settings: STD and HSD fed-batch processes. The processes were performed using CHO cell cultures as CHO cells are the preferred host for antibody production on the manufacturing scale [2]. Measured data were used to calculate the specific growth rate and the specific production or release rate of metabolites and antibody products; these data were then used for segmented modeling. The experiments and analytics are described in Section 2: Material and Methods. The data analysis and modeling are described in Section 3: Data Analysis and Mathematical Models. Furthermore, an average model is generated using the segmented linear regression approach, which describes the cellular behavior of each metabolite and therefore is used to improve specific feeding. This paves the way towards more streamlined optimizations of the feeding regime in the process due to deeper insights into the metabolism of cells in HSD processes. To upgrade the methodology, we utilized a metabolic flux analysis (MFA) to calculate the intracellular fluxes.

The objectives of this study can be clearly defined into three areas:

1. Analysis and comparison of metabolic phases in conventional and high seeding density processes using segmented modeling.
2. Application of a segmented model for feeding optimization with the HSD process using measured experiments.
3. Metabolic flux analyses and extension of segmented modeling by integration of intracellular fluxes.

2. Materials and Methods

2.1. Cell Lines, Seed Train and Cultivation Processes

A proprietary CHO-K1 GS cell line producing a monoclonal antibody was cultivated in a chemically defined, in-house-developed medium. The cell line was originally derived from ATCC depository cell bank CCL-61 and is devoid of functional alleles for the glutamine synthetase gene (CHO-K1 GS). The cell line development has already been described in the work by Stadermann et al. [9].

The cells were thawed in the N-7 stage and then further cultivated until the N-3 stage in shake flasks. The cells were cultivated in the whole seed train at 36.5 °C and 5% CO_2 and the shake flasks were agitated at 120 rpm and 50 mm orbit. Cells were then transferred into a 10 L wave (Flexsafe® RM, Sartorius, Gottingen, Germany) in the N-3 stage. The wave stage was agitated by 24 rocks/min at a 7° angle. The seeding cell density of the process was set to 0.5×10^6 cells/mL for three day passages and to 0.7×10^6 cells/mL for two day passages.

The N-2 stage was the first controlled bioreactor process in the seed train. Here, the cells were cultivated in an 8 L bioreactor for three days in a batch process. The seeding cell density of the process was set to 0.4×10^6 cells/mL. The medium was equilibrated for 24 h before inoculation. Cells were cultivated at 50% pO_2, 6.95 ± 0.15 pH, 36.5 °C and 176 rpm. The N-1 stage was conducted in 4 L bioreactors for 6 days as a perfusion process. Cells were retained with tangential flow filtration (TFF) by using single-use, customized flow paths (MiniKros®, Repligen, Waltham, MA, USA) consisting of a modified polyethersulfone (mPES) membrane with a 0.65 µm pore size. A perfusion system from Repligen (KrosFlo® KML™50, Waltham, MA, USA) with a centrifugal pump was used to control a constant recirculation flow over time. The perfusion rates were adjusted every 24 h by the reactor volumes per day. The seeding cell density of the process was set to 0.8×10^6 cells/mL. The

medium was equilibrated for 24 h before inoculation. Cells were cultivated at 40% pO_2, 6.95 ± 0.25 pH, 36.5 °C and 200 rpm. The pH was controlled using 1 M carbonate and CO_2 gassing; the foaming was controlled by addition of antifoam as required.

Both different N-Stage fed-batch processes (HSD and STD) were inoculated by using N-1 perfusion and were conducted in 3 L glass bioreactor systems (Applikon Biotechnology). The seeding cell density (SCD) of the STD process was 0.7×10^6 cells/mL and the SCD of the HSD process was 10×10^6 cells/mL. Both process types are illustrated in Figure 1. The cultivation duration was up to 14 days. Process parameters, such as pO2, temperature, pH and P/V, were identical in both process types. Cells were cultivated at 50% pO_2, 6.95 ± 0.25 pH, 34.5 °C and 263 rpm. The pH was controlled using 1 M carbonate and CO_2 gassing; the foaming was controlled by the addition of antifoam as required. The feed medium was added in both processes continuously until harvest; however, feed start was on day zero for the HSD process and on day one for the STD process. The feeding strategy started at 45 mL/L/day and was changed on day nine to 25 mL/L/day. If the glucose concentration was below 3 g/L, glucose was added to reach a 5 g/L glucose concentration. If indicated, a bolus was added to the HSD N-Stage processes. The processes HSD LAC and HSD CYS were supplemented with sodium lactate (day 3 to 13; bolus criteria: ≤2 to 3 g/L) or cysteine (fixed bolus: 7 mL from day 1 to day 5), respectively. Sodium lactate and cysteine were both added with the already described criteria to the HSD LAC/CYS process. The addition of lactate and cysteine are already described in the patent WO2021165302A1 [10]. Similar seed train and cultivation processes were performed by Brunner et al. [5].
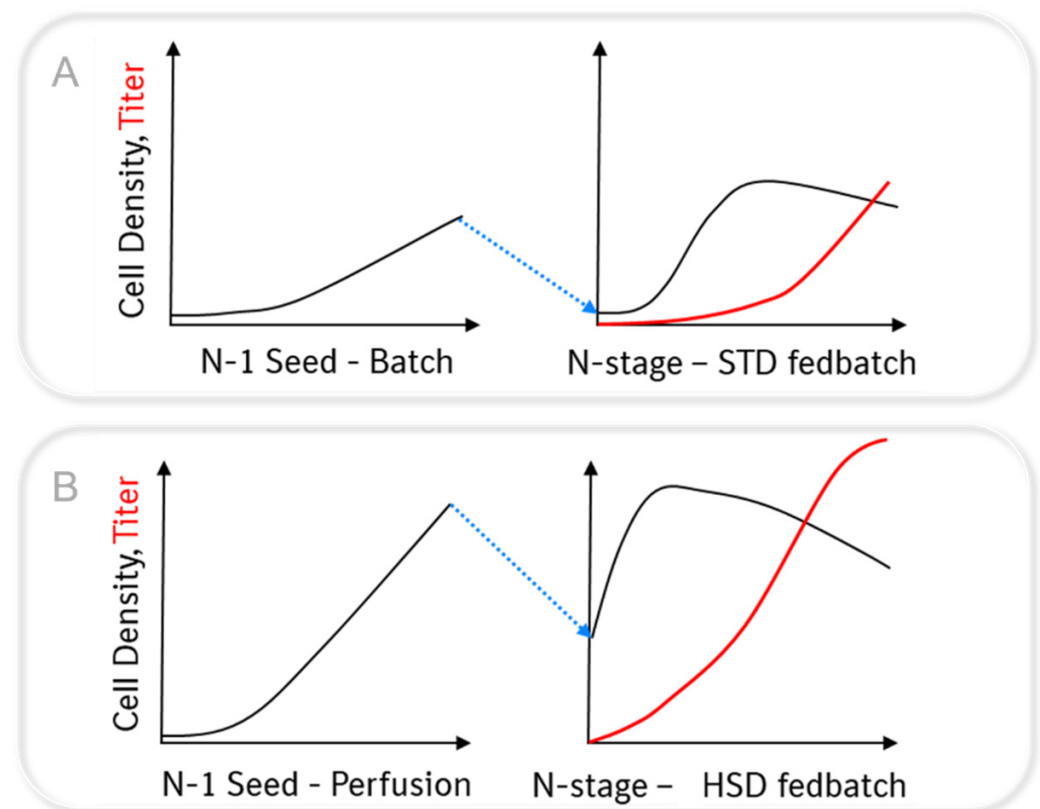

Figure 1. Illustration of N-1 prestage and N-Stage of the conventional standard (STD) process (**A**) and high seeding density process (**B**). The STD fed-batch N-Stage is inoculated with a batch N-1 stage, while the HSD fed-batch N-Stage is inoculated with an N-1 perfusion stage, where cells are retained through a filter module to reach high cell densities. Black color line describes cell density and red line describes titer. Blue dotted arrow describes transfer from N-1 into N-Stage.

2.2. In-Process Analytics

Samples were taken in the seed train in shake flasks and wave stages at transfer day and these were analyzed for cell count, glucose and lactate concentration. In the controlled prestages and the N-Stage, samples were taken every 24 h. Samples were analyzed in N-2 stage for cell count, glucose, lactate and ammonia. The following parameters were analyzed in the N-1 and N-Stage: cell count, glucose, lactate, ammonia, osmolality, antibody concentration and amino acids.

The viable cell density and viability were measured using a Cedex HiRes analyzer (Roche) and the corresponding software Cedex Software Version 2.3.4 for the device. The viability was determined using trypan blue. Metabolites were measured with a Konelab™ Prime60i (Thermo Fisher Scientific, Waltham, MA, USA) device. The measuring principle of the Konelab™ Prime60i is based on photometric measurements. The samples were mixed with reagents and an enzymatic reaction took place.

A Protein-A HPLC method (Thermo Fisher Scientific) was used to measure antibody concentration. The antibody concentration measurement was based on the principle of affinity chromatography, where the matrix is silica gel and the ligand is protein A. The used column was from Applied Biosystems (PA Immuno Detection Sensor Catridge 2.1 mm (ID) × 30 mm). The following parameters were used for the antibody concentration measurement: flow: 2 mL/min; wavelength: 280 nm; runtime: 7 min; and buffer with mobile phase A (pH 7.4) and mobile phase B (pH 2.6). Amino acids were measured with a 7890B GC System (Agilent Technologies) using the EZ faast Kit from the supplier Phenomenex. Cysteine measurements were excluded due to stability issues [11,12]. Similar analytics were performed by Brunner et al. [5].

3. Data Analysis and Mathematical Model

3.1. Metabolic Steady State

In general, metabolic phases are defined by a metabolic steady state. As a consequence, intracellular concentrations remain constant within a phase as stated by Yahia et al. [13,14]. It is further assumed that when all intracellular concentrations remain constant, the metabolic fluxes as well as yield coefficients are also constant [14,15]. The basis for phase identification is the presumption that consumption of substrates is separated into two parts: A part of the consumption is growth-associated and therefore proportional to the specific growth rate, μ. The other part is not consumed in association with growth and is used for maintenance purposes or for the synthesis of non-growth-associated products [16]. The production of the biopharmaceutical product can either be coupled with growth or modelled independently from growth [17]. Based on this theory, an equation was formulated for the substrate consumption (S) and product formation (P):

$$\begin{bmatrix} r_s \\ r_p \end{bmatrix} = A * \mu + B = \begin{bmatrix} a_s \\ a_p \end{bmatrix} * \mu + \begin{bmatrix} b_s \\ b_p \end{bmatrix} \tag{1}$$

It was previously assumed that fluxes remain constant per phase, and, as shown in Equation (1) as a linear function, *A* and *B* are constant within a metabolic phase. The practical consequence of this is that the specific rate of production or release of metabolites and antibody products can be expressed as a function of the growth rate. This is done by using joined linear sub-models for the distinct metabolic phases. The breakpoints between linear sub-models then correspond to metabolic shifts that connect metabolic phases [14].

3.2. Phase Identification

For phase identification, the vector *A* is further used and assumed to be constant. The value of *A* is calculated by using the derivative of Equation (1). As the derivative can amplify analytical and biological inaccuracies, the data of specific rates were first cleaned with the ROUT method (performed with GraphPad Prism). Briefly, the ROUT method is based on a model that is fitted to the data. This is performed with a robust method where

outliers have little impact. Then, a new outlier detection method is used to detect outliers. These are data points that are far enough from the prediction of the model [18]. Then, the data were smoothed as a function of the specific growth rate using the LOWESS method (linear locally weighted scatterplot smoother) with the software GraphPad Prism. This was followed by the calculation of vector *A* by using the derivation of LOWESS. LOWESS and all following data analysis steps were performed using JMP® (SAS institute).

In the next step, the aim is to find the values of *A* with small variation, as these were assumed to be constant within a phase. This step was performed with recursive partitioning. This method splits the derivatives of all metabolites into sub-populations according to a splitting value. The splitting value maximizes the -log(*p*-value)—also called log worth—of the chi-square test. This is done to measure how different the data are in the two partitions. These partitions are determined to identify the number of breakpoints. To identify the metabolic phases for all metabolites, hierarchical clustering was used to find similar breakpoints. The agglomerative procedure, called Ward's method [19], was used for clustering. First, each measurement starts in its own cluster. Then, the distance of each cluster is calculated and the nearest clusters are merged. The decision on the final number of clusters is based on the first knee point in the linkage function. The knee point is defined as the peak in the second-order derivative of the linkage distance function. This results in the identification of the metabolic phases as the breakpoints between phases. The workflow for identification of metabolic phases together with the segmented modelling approach (Section 3.3) has already been published by Yahia et al. [14] and is shown in Figure 2.
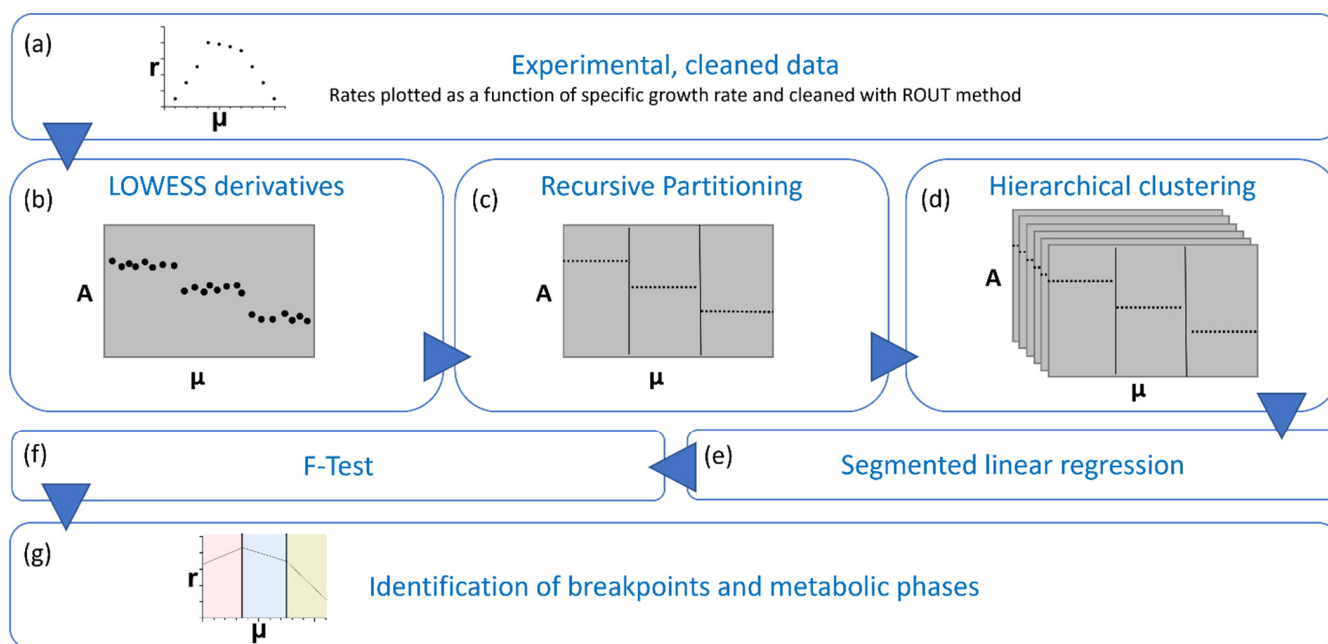

Figure 2. Workflow for identification of metabolic phases with the segmented modeling approach (modified process of Yahia et al. [14]). (**a**) Raw experimental data of specific rates were plotted as a function of specific growth and then were cleaned with the ROUT method. (**b**) The data were smoothed with the LOWESS method and the derivatives of LOWESS were calculated. (**c**) Recursive partitioning was used to split all calculated derivatives of each metabolite into sub-populations. (**d**) Similar breakpoints were identified with hierarchical clustering. The final number of clusters selected was chosen as the first knee point in the linkage function. (**e**) Segmented modeling is a method in which the specific growth rate is partitioned into intervals and each interval is modelled using linear regression. The breakpoints used in the segmented linear regression were the values of the two line segments intersections. (**f**) The segmented modeling process was analyzed with the F-Test to avoid overfitting and to reduce the number of breakpoints if this makes the model statistically superior. (**g**) With the F-Test, the final number of breakpoints and therefore the metabolic phases are identified.

3.3. Segmented Modeling

Segmented modeling—also referred to as segmented regression—is a method in which the independent variable (in this case μ) is partitioned into several segments and then each interval is modelled using linear regression [20]. The breakpoints are used as the values where the two line segments intersect. To avoid overfitting, the resulting segmented regression is analyzed with an F-test to determine whether the addition of a breakpoint makes the model statistically preferable to a model with a reduced number of breakpoints (Figure 2). The F-Test and segmented modeling were performed with GraphPad Prism.

3.4. Metabolic Flux Analysis

Metabolic flux analyses provide deeper insights into cell metabolism. Here, we use an MFA for the determination of significant metabolic pathways in the metabolic model; intracellular fluxes are calculated by utilizing a stoichiometric model for the major intracellular reactions and by applying mass balances around intracellular metabolites [21]. A metabolic flux analysis was performed with MATLAB 2019a and the toolbox PFA. The PFA toolbox provides a comprehensive set of MATLAB functions to apply possibilistic MFA. Possibilistic MFA can handle inconsistencies by considering sensor errors and model imprecision to provide rich and reliable flux estimations [22]. A metabolic network of the central carbon metabolism of CHO cells was applied based on published works [23,24]. The network comprised glycolysis, pentose phosphate pathway (PPP), the TCA cycle and amino acid metabolism. Compartmentation was neglected. Specific rates of consumption or release of metabolites at sampling were used as model inputs. Th specific oxygen uptake rate was not measured; therefore, an estimation was used. Xing et al. [25] measured the specific oxygen consumption to be 0.32 pmol/cell * h in CHO cells. As this was measured in a different system with different conditions, a standard deviation of 20% was used. In the next phase, the calculated intracellular fluxes were coupled with the measurements to enrich the dataset for the identification of metabolic phases.

4. Results and Discussion

4.1. Process Performance: Standard vs. High Seeding Density Fed-Batch

To investigate the impact of intensified fed-batch processes compared to standard fed-batch (STD) processes, different seeding cell densities, such as 0.7×10^6 cells/mL (STD), and high seeding densities (HSD) with 10×10^6 cells/mL were employed (Figure 3). The idea behind an intensified fed-batch process is that the accumulation of cell mass in the production stage is shifted into the N-1 expansion stage by using perfusion [7]. This desired effect can be seen in the experimental data of STD and HSD processes. The accumulation of the cell mass in the HSD process is shifted largely into the prestage, as the HSD process reaches its peak viable cell density five days earlier than the STD process. There are two further differences between HSD and STD processes: the HSD process reaches a higher peak VCD and the viability declines earlier. The characteristics of an intensified process as seen in our runs were also observed by Padawer et al. [26]. A low viability can significantly affect product potency and quality [27]. Product quality plays a pivotal role in bioprocesses; hence, increasing the harvest viability is an important development goal. Therefore, the problem of reduced viability in HSD processes must be addressed.

There are different approaches to increase the harvest viability, e.g., by process parameters such as temperature or by improving media supplementation. This work will focus on the media platform. Therefore, two supplementations, lactate (LAC) and lactate + cysteine (LAC + CYS), were tested, as these have already been described in the literature [5]. The HSD10M + LAC process and the HSD10M process without additions showed similar behavior for viable cell density and for viability. The addition of LAC and CYS led to a higher viability and therefore to a higher viable cell density.

The HSD process reached a ≈ 33% higher titer compared to the STD process. The supplementation of LAC did not improve the productivity. However, supplementation of LAC + CYS led to a significant increase of about 57% in the titer compared to the

HSD process without supplementation. This increase is due to a sustained viability and thus higher integral of viable cells (IVC), in addition to a higher cell-specific productivity. Therefore, the final product titer of the intensified process with LAC + CYS supplementation was ≈110% higher than the standard fed-batch process. The addition of lactate to our in-house combination with CYS might be beneficial for increasing cell-specific productivity. Cysteine has also been shown to improve cell viability by an increase in the intracellular glutathione concentration, thereby actively reducing reactive oxygen species (ROS) [5,10,28].
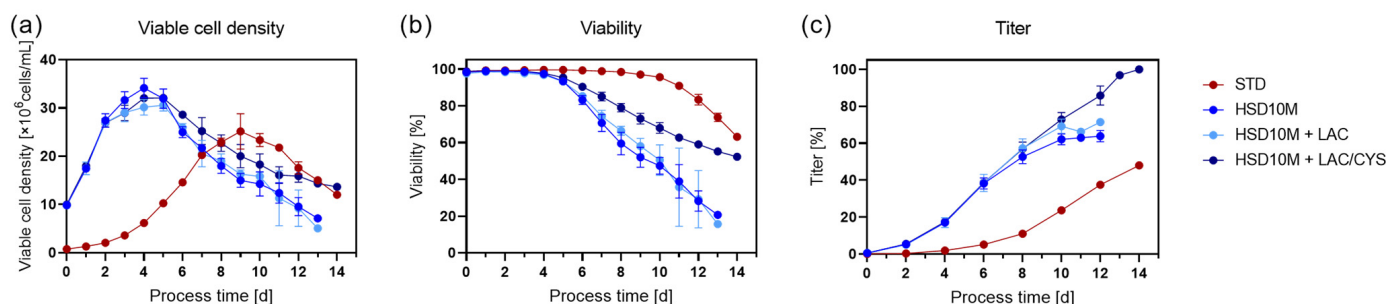

Figure 3. (**a**) Viable cell density, (**b**) viability and (**c**) titer (normalized) over process time (in days) for the investigated processes: standard (2), HSD10M without supplementation (5), HSD10M with LAC supplementation (3) and HSD10M with LAC/CYS (2) supplementation. All experiments were conducted at least twice ($n \geq 2$). The numbers in the brackets show the number of runs which were used for this analysis. STD, standard process with seeding density of 0.7×10^6 cells/mL; HSD10M, process with the seeding density 10×10^6 cells/mL; +LAC, supplemented with lactate; +LAC/CYS, supplemented with lactate and cysteine.

4.2. Identification of Metabolic Phases Using Extracellular Fluxes

The extracellular environment is always changing due to consumption of substrates and the accumulation of waste products. Cells are constantly adapting to this changing environment and this results in different metabolic phases. The shifts between phases indicate the time point at which cells enter a new metabolic phase. Therefore, these phases must be identified first to provide an understanding of the phenotypic behavior of cells and to propose strategies for the optimization of HSD processes [29]. Focusing only on growth phases (including the lag phase, exponential phase, and stationary phase) may result in metabolic shifts that can be only detected by observing the yield coefficients between metabolite consumption and cell growth being missed. Therefore, we employed the approach of segmented linear regression described by Yahia et al. [15] to identify metabolic phases. This method circumvents the described problem by the application of a metabolic steady state concept. In such a state, specific metabolite rates remain constant within a metabolic phase [14]. We applied segmented regression on the cleaned datasets containing specific growth rates and specific production or consumption rates of metabolites and recombinant antibodies. We performed segmented modeling on the STD process and HSD10M, HSD10M + LAC and HSD10M + LAC/CYS process types.

4.2.1. Comparison of Identified Breakpoints

Segmented modeling results in the identification of breakpoints; these breakpoints describe when cells enter a new metabolic phase. Figure 4 describes the identified breakpoints for the different process types. Each breakpoint is described in terms of the corresponding specific growth rate to provide a better understanding. The first breakpoint describes the change from the 1st to the 2nd metabolic phase; the value of the first breakpoint decreases from the STD process to HSD10M, HSD10M + LAC and finally to HSD10M + LAC/CYS. The second breakpoint describes the change from the 2nd to 3rd metabolic phase; it occurs at higher specific growth rates in the STD process compared to the other process types. The decrease in the specific growth rate in which the breakpoint is identified from the first into the second metabolic phase correlates with an increasing final titer concentration. This

cannot be seen in the second breakpoint. These results may be explained by the observation that the first metabolic phase is characterized by cell growth, while the second and third phases are characterized by a titer increase. Therefore, an earlier shift from phase 1 to phase 2 may be relevant for the final titer in contrast to the transition from phase 2 to phase 3.

(a)

1st breakpoint [1/d]	
Standard	0.384
HSD10M	0.221
HSD10M + LAC	0.208
HSD10M + LAC/CYS	0.160

Decreasing specific growth rate, at which the phase change from P1 to P2 occur

(b)

2nd breakpoint [1/d]	
Standard	0.035
HSD10M	−0.084
HSD10M + LAC	−0.015
HSD10M + LAC/CYS	−0.047

Lower specific growth rate, at which the phase change from P2 to P3 occur

Figure 4. Comparison of identified breakpoints with the method segmented linear modeling for the processes: standard (2), HSD10M without supplementation (5), HSD10M with LAC supplementation (3) and HSD10M with LAC/CYS (2) supplementation. The number in the brackets shows the number of runs which were used for this analysis. First breakpoint is shown in (**a**) and the second breakpoint is shown in (**b**). STD, standard process with seeding density of 0.7×10^6 cells/mL; HSD10M, process with the seeding density 10×106 cells/mL; +LAC, supplemented with lactate; +LAC/CYS, supplemented with lactate and cysteine. The light blue arrow shows that the value of the first breakpoint decreases from the STD process to HSD10M, HSD10M + LAC and finally to HSD10M + LAC/CYS. The dark blue arrow shows that the second breakpoint is at higher specific growth rates in the STD process compared to the other process types with HSD10M.

4.2.2. Comparison of the Growth Behavior and Length of Identified Phases

The phase change in the HSD processes mostly occurs on the same process days, as shown in Figure 5. These phase shifts are around day three and between days five and six. However, the phase shift for the STD process is different and occurs around day six and around day nine. The phase duration in the HSD processes for the first two phases is ≈ three days, while the third phase is ≈ eight days long. This differs from the STD process, where the first phase is six days long, the second phase is three days and the third phase is five days long. Therefore, the first phase is shortened by three days in the HSD10M processes, while the third phase is prolonged by three to four days compared to the STD process. Figure 3 demonstrates that when the phase shifts occur earlier in the process, the specific productivity increases and therefore benefits the overall titer in the different HSD processes. Yang et al. also showed [7] that shifting the growth phase in the N-1 phase by using a higher seeding density leads to a higher volumetric productivity.

These data show that the HSD process is shifted by three days. The first phase is known for biomass production. Therefore, the higher seeding density leads to a partial shift in the cell growth phase away from capital-intensive large-scale reactors into the smaller previous stage [30]. However, when looking at the different trends in amino acids and metabolites in each phase between the STD and HSD processes (data shown in Section 4.2.3), not only is the process shifted by three days, but the data also suggest differences within the phases.

The duration of the metabolic phases of the HSD processes are similar; however, the HSD + LAC/CYS process has a slightly longer second phase than the other HSD processes. The second phase is characterized by lactate consumption, as discussed later. Lactate consumption is favorable for the process [31]; therefore, this prolongation of the

second phase could be a potential reason for the improved process performance of the LAC/CYS process.
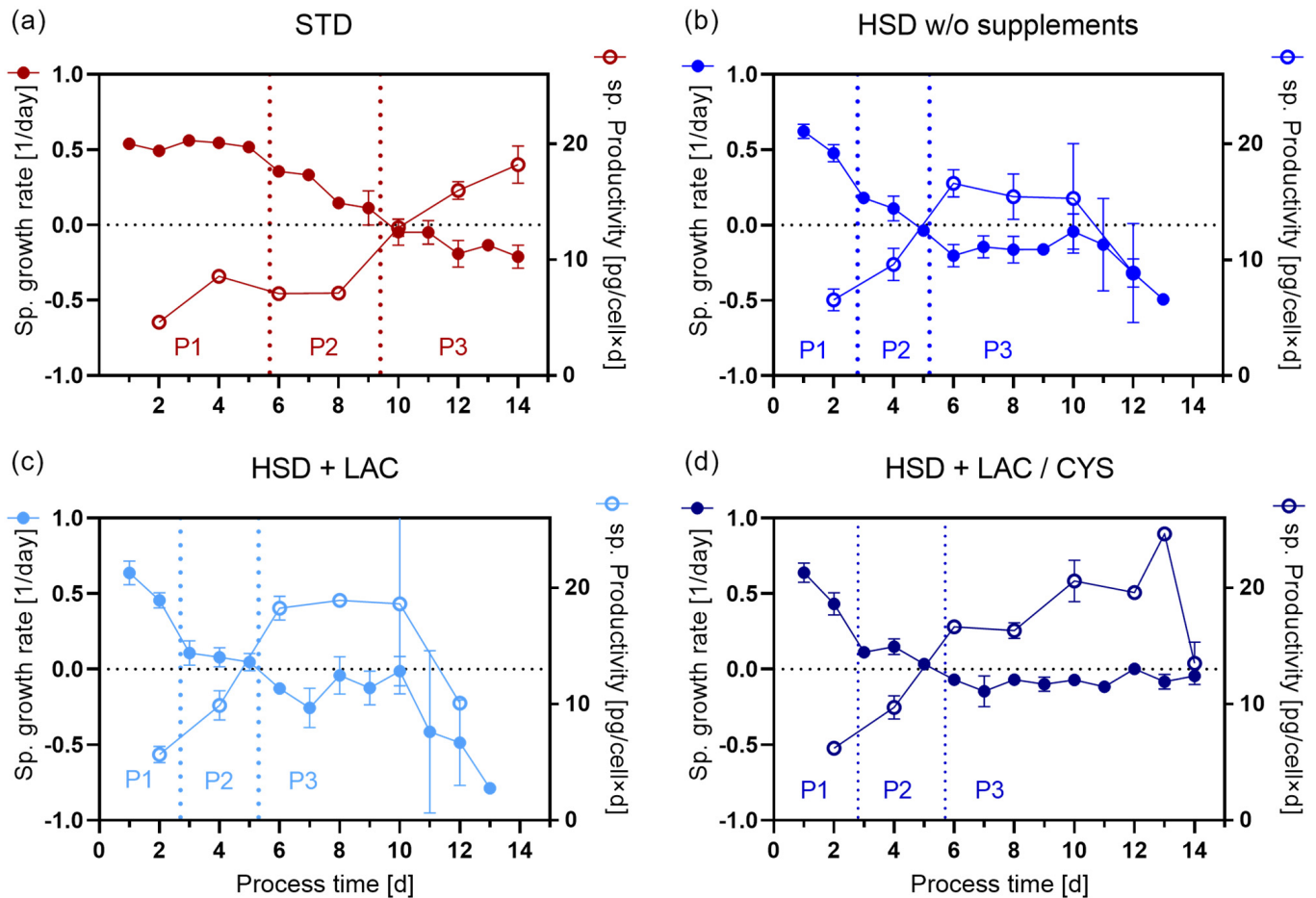

Figure 5. Illustration of identified phases with the data of specific growth rate and specific productivity against the process time for the processes: (**a**) standard (2), (**b**) HSD10M without supplementation (5), (**c**) HSD10M with LAC supplementation (3) and (**d**) HSD10M with LAC/CYS (2) supplementation. The number in the brackets behind the process types shows the number of runs which were used for this analysis. STD, standard process with seeding density of 0.7×10^6 cells/mL; HSD10M, process with the seeding density 10×10^6 cells/mL; +LAC, supplemented with lactate; +LAC/CYS, supplemented with lactate and cysteine.

4.2.3. Comparison of the Rates in the Identified Phases

Figure 6a presents the models of productivity and the most important metabolites: glucose, lactate and ammonium. There are differences between the processes regarding the metabolism of glucose and lactate. For all processes, glucose consumption occurs during the whole process, while the highest consumption is in the first phase. When comparing the rates among the process types, the STD process has the highest glucose consumption rate and the highest lactate production rate in the first phase. In conclusion, the STD process consumes more glucose and produces more lactate at similar growth rates. These differences likely relate to the cells' different stages. Vodopivec et al. [32] presented different metabolite characteristics (including glucose and lactate) in the growth stages and early and late exponential growth phases. This suggests that the STD process is in the early exponential growth phase, while the HSD processes are already shifted to the late exponential growth phase with a reduced need for glucose. When only considering the different HSD processes, a similar trend in these metabolites is visible. This confirms that supplementation does not lead to an altered glucose/lactate metabolism.
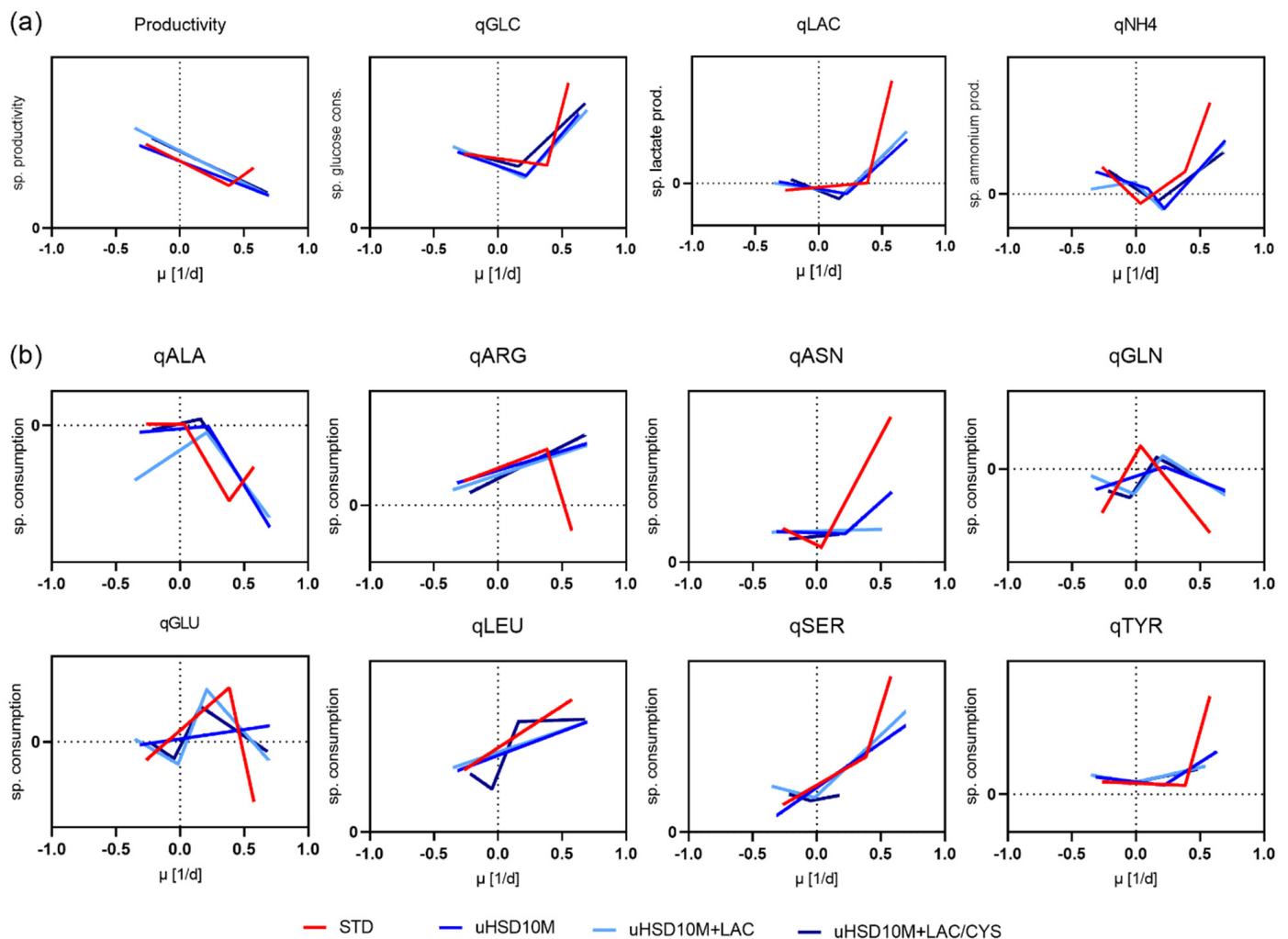
Figure 6. Comparison of segmented linear modeling for productivity and specific rates of consumption or release of glucose, lactate and ammonium (**a**) and for selected amino acids (**b**) for the processes: standard (2), HSD10M without supplementation (5), HSD10M with LAC supplementation (3) and HSD10M with LAC/CYS (2) supplementation. The number in the brackets shows the number of runs which were used for this analysis. Data points were cleaned before segmented modeling; therefore, some models are reduced, e.g., for the model of qSer for HSD10M + LAC/CYS. Some models resulted in less than three phases due to the F-Test, which avoids overfitting. ALA = alanine; ARG = arginine; ASN = asparagine; GLN = glutamine; GLU = glutamate, LEU = leucine; SER = serine; TYR = tyrosine. The prefix q describes the specific rates of consumption or release. STD, standard process with seeding density of 0.7×10^6 cells/mL; HSD10M, process with the seeding density 10×10^6 cells/mL; +LAC, supplemented with lactate; +LAC/CYS, supplemented with lactate and cysteine.

The segmented models of the productivity for HSD without additions and the STD process are almost identical for most μ values. This suggests that a higher seeding density did not alter productivity. Only a higher cell number led to a higher titer. The addition of LAC and LAC/CYS slightly increases the slope of the trend line. The specific productivity increases with these supplementations.

The uptake rates of the amino acids per phase are shown in a heatmap (Figure 7). The rates of most of the amino acids, for example, LYS, MET, PHE and VAL, are similar for all processes. They only show a moderate exchange flux between the different process types. However, some amino acids show clear differences between the process types (models shown in Figure 6b).
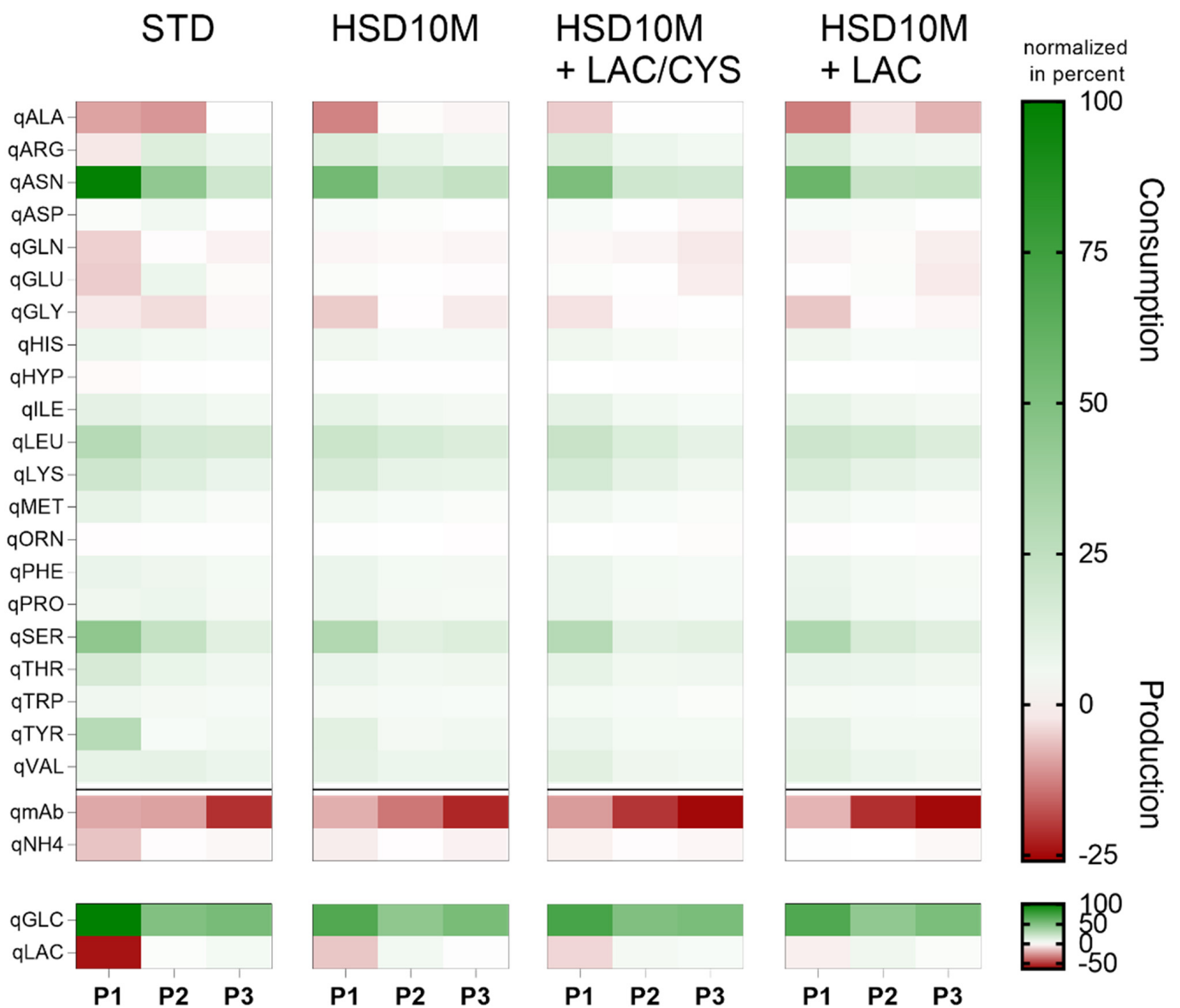
Figure 7. Heatmap of the median consumption and production of the amino acids, glucose, lactate and ammonium, and productivity. The phases of each process type were identified with segmented linear modeling for the processes: standard (2), HSD10M without supplementation (5), HSD10M with LAC supplementation (3) and HSD10M with LAC/CYS (2) supplementation. The number in the brackets shows the number of runs which were used for this analysis. STD, standard process with seeding density of 0.7×10^6 cells/mL; HSD10M, process with the seeding density 10×10^6 cells/mL; + LAC, supplemented with lactate; + LAC/CYS, supplemented with lactate and cysteine. ASP = aspartate; GLY = glycine; HIS = histidine; HYP = hydroxyproline; ILE = isoleucine; LYS = lysine; MET = methionine; ORN = ornithine; PHE = phenylalanine; PRO = proline; TRP = tryptophan; TYR = tyrosine; VAL = valine; mAb = monoclonal antibody. The prefix q describes the specific rates of consumption or release.

 The highest consumed amino acid was asparagine. Asparagine (ASN) is an important non-essential amino acid in cell culture media, playing a central role in key metabolic pathways [2,33]. CHO cells tend to highly consume asparagine compared to other amino acids, as ASN is used to replenish the TCA cycle [2]. The STD process showed a higher consumption in phase one and two. As Ritacco et al. [2] reported, ASN is mostly consumed in the exponential phase. During cultivation, the specific growth rate declined, as did the as-

paragine uptake, which confirms the statement of Ritacco et al. STD cultivations displayed elongated higher consumption, which correlates with their extended growth phase.

Comparing the different models of asparagine, the trendline of asparagine has a higher slope at high growth rates for the STD process compared to the HSD processes. Therefore, the increased consumption of ASN in the STD process is a major reason for the increased ammonia production (Figure 7). As mentioned before, the increased uptake shows that the HSD process is not just shifted in time, but also the metabolism is altered. This can also relate to differences in the early and late exponential growth phases as already stated by Vodopivec [32].

Similar observations to ASN were made for SER. Serine is an important amino acid involved in the provision of precursors and co-factors for nucleotides biosynthesis. In proliferating cells, increased nucleotide synthesis is necessary for DNA replication and for RNA production to enable protein synthesis at different stages of the cell cycle [34]. This correlates with the observed higher uptake rates of serine in the exponential phase for all processes and with the highest uptake rate in the STD process. At these points, the cells were in the beginning of the exponential growth phase (Figure 6b). The data were cleaned before segmented modeling; therefore, some of the models are reduced where a higher amount of data were excluded, e.g., qSer for HSD10M + LAC/CYS.

Alanine, besides lactate, is the highest produced metabolite. According to Li et al. [35], alanine typically accumulates during the rapid early growth stage of cell cultures and is produced after nitrogen detoxification [36]. This can be seen in the model, as the production rate is the highest for all processes at high growth rates. The alanine production is shut down on day three for HSD runs and on day nine for STD processes. This correlates with the metabolic shift to lactate consumption. The glycolytic flux is not sufficient anymore to fill the TCA cycle and presents a probable reason why lactate is consumed and why alanine is not produced anymore.

4.3. Feed Optimization Using Segmented Modeling

Feed optimization mostly relies on lab experiments based on design of experiments (DoE). To reduce the number of experiments in the design space, the segmented model provides a guidance on cell-specific demands. Therefore, an average segmented model was calculated with a broader design space. The average model consists of the data from the three different HSD runs, which are merged to obtain a larger dataset including 29 HSD processes. The data were used to calculate the mean and 3SD. This average model was then validated by further using a dataset (HSD process with LAC/CYS supplementation) which was not used for the model. The average model was used for feed optimization. For this purpose, we compared the average model calculated with specific rates with the specific feeding of the respective metabolite (glucose and lactate) and for the amino acids (Figure 8). The benefit of segmented modeling in this feed optimization is the simplified approach to generate an average model that considers the metabolic phases. Here, we applied two different approaches for the optimization of the feeding regime.

4.3.1. Reduction in Overfeeding

A comparison of the average consumption model and the specific feeding shows an overfeeding of most of the amino acids between day six and day nine. The amino acids were arginine, histidine, isoleucine, leucin, lysine, methionine, phenylalanine, proline, serine, threonine, tryptophane, tyrosine and valine. A similar trend can be seen for each of these amino acids. The specific consumption model stays at a lower level, while the specific feeding is increased due to a constant feeding rate and a reducing viable cell density. From day nine onwards, the feeding rate is reduced. The overfeeding starts at day six; this correlates with the metabolic shift that was observed above. Therefore, a feeding rate change at the timepoint of a predicted metabolic shift would be effective to prevent overfeeding.
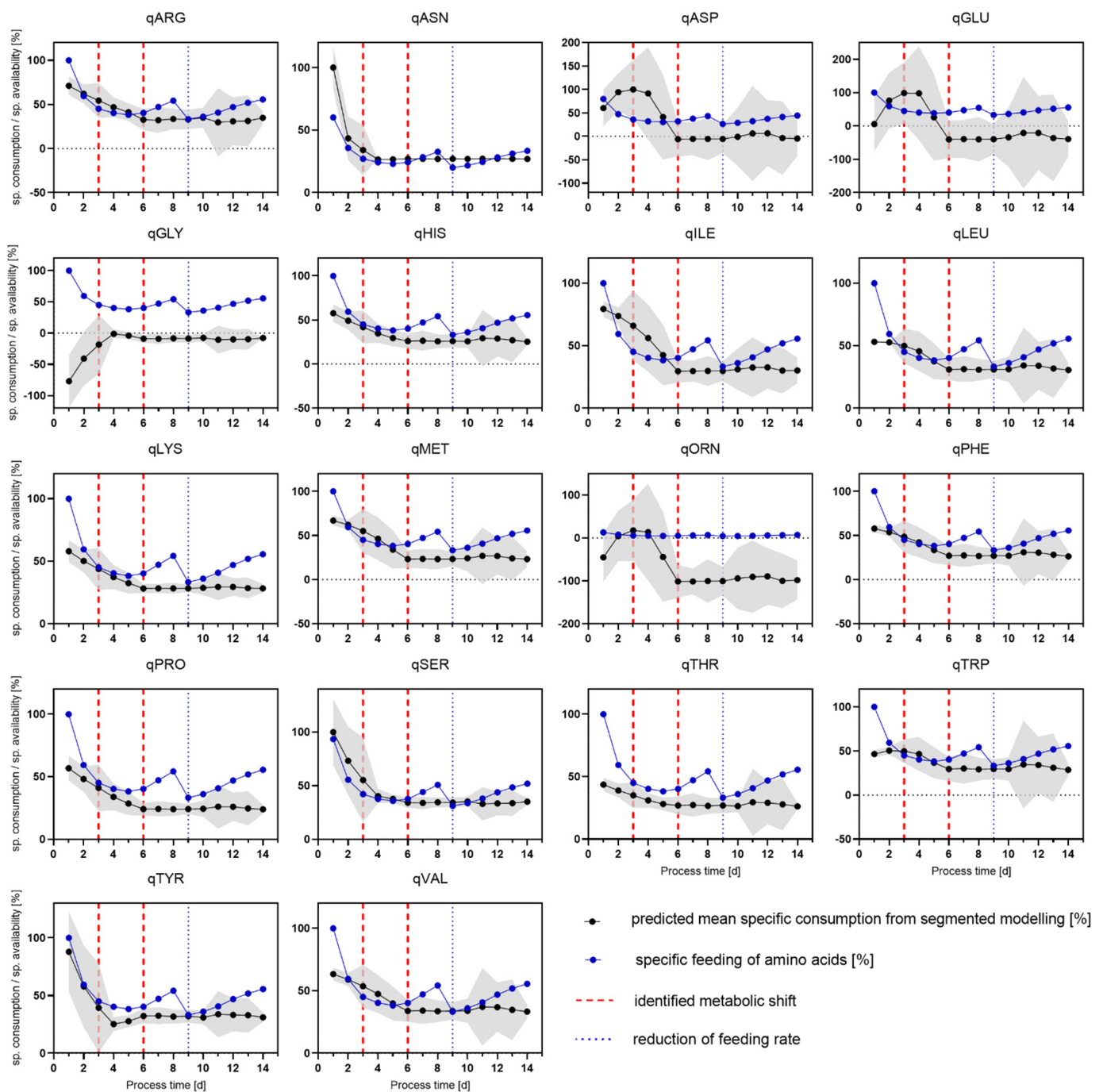
Figure 8. Comparison of predicted mean specific consumption from segmented modeling (average model which comprised three different HSD processes) with the specific feeding of amino acids. The identified metabolic shifts are depicted in red and the reduction in the feeding rate is shown in blue.

Brunner et al. [5] published their work focusing on HSD processes and applied an extended metabolite analysis. An analysis of cultivation samples revealed the potential of inhibiting metabolites accumulating in the HSD and STD culture at the timepoint when cell viability started to decrease. These potential inhibiting metabolites, such as 2-deoxycitidine, indole-3-lactic acid, indole-3-carboxylic acid and 2-hydroxybutyrate, accumulate early in HSD cultures. Mulukulta et al. [37] analyzed these metabolites and further inhibitory substances, i.e., catabolic intermediates or by-products of phenylalanine, tyrosine, tryptophan, leucine, serine, threonine, methionine or glycine metabolism. Overfeeding of amino acids may therefore lead to an accumulation of these inhibitory substances.

The feed composition was developed in-house to meet nutrient needs during cell culture. Changing the feed composition in the bioprocess is highly complex and not a common practice. However, eliminating the overfeeding between day six and day nine in the HSD processes by reducing the feed rate earlier is easy to implement in the lab.

In order to validate the hypothesis of earlier feed reduction based on in silico observations, we performed a complementary study with the preliminary investigated cell line and a further cell line. The results from this study can be seen in Figure 9. The titer at harvest day did not significantly change between the control and the reduced feed. There is only a slight improvement in the viability of $\approx 6\%$ on the last process day. The reduction in the feed led only to a marginal improvement in the process. However, the results support the segmented model as a suitable method for feed optimization. The reduction in the feed did not lead to a depletion or to an inferior process performance and intense overfeeding was eliminated.
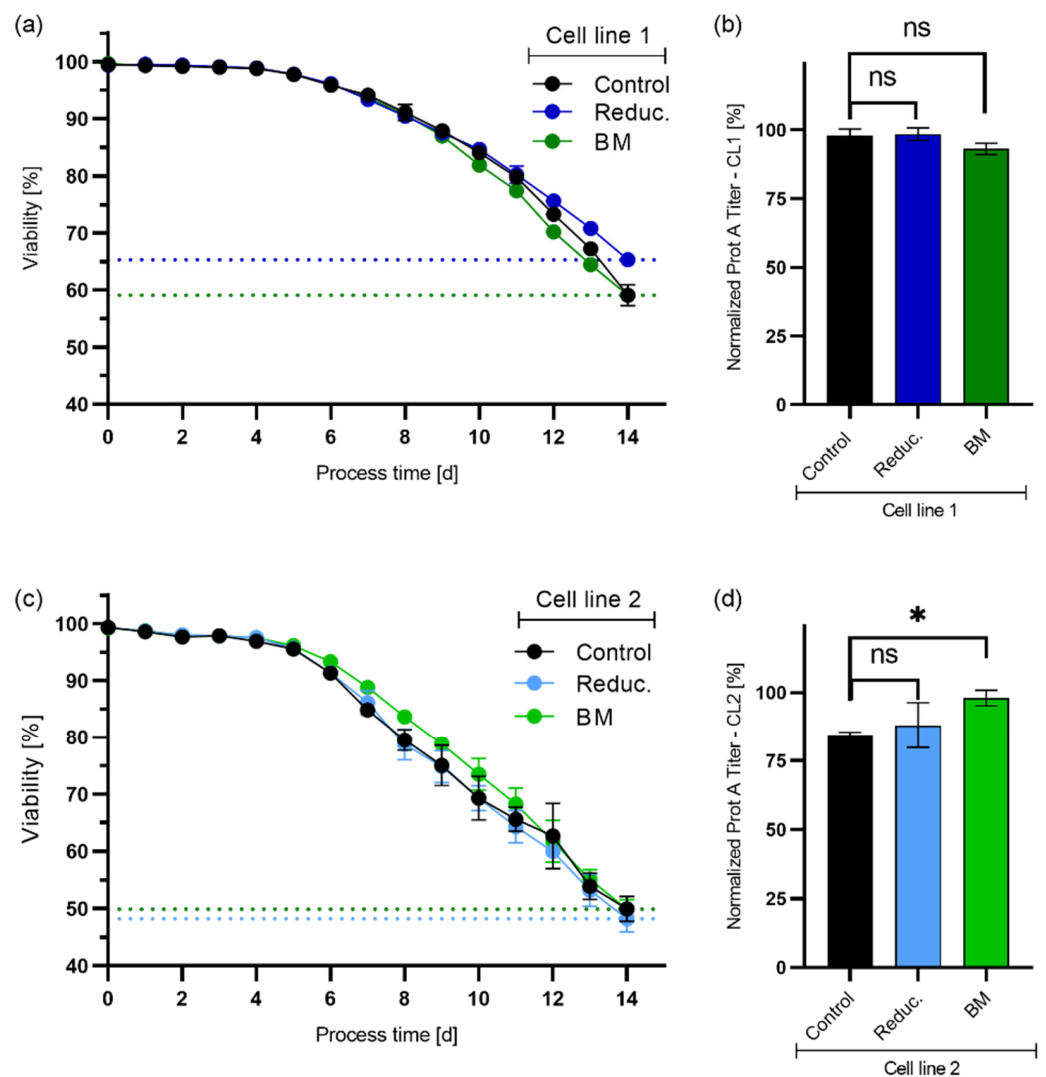

Figure 9. (**a**,**c**) Viability and (**b**,**d**) pre-harvest titer (normalized) for the cell line 1 (**a**,**b**) and cell line 2 (**c**,**d**) with the comparison of three processes: the HSCD10M control process (black), the HSD10M process with an earlier reduction in the feeding rate (denoted Reduc. in blue) and the HSD10M process with addition of bolus media (on process day 0–5) with the amino acids asaparagine, aspartate, glutamate and isoleucine (denoted BM in green). The processes were performed in duplicate ($n = 2$). An unpaired *t*-test was performed for the Prot A titer at harvest. n.s. means not significant, * means $p \leq 0.05$.

4.3.2. Addition of Depleted Amino Acids

In the second approach, the average model and the specific feeding strategy were used to detect which amino acids have a significant difference between feeding and consumption; this difference will indicate which amino acids are underfed. The most prominent example of a depleted amino acid is asparagine (ASN). ASN is used to replenish the TCA cycle and has been reported to be a key amino acid that could potentially suppress apoptosis. ASN and three other depleted amino acids, aspartate, glutamate and isoleucine, were formulated in a stock solution and were given as bolus in metabolic phases one and two from day 0 to day 5 in a complementary study. The resulting titer is shown in Figure 9. The bolus addition showed a significant titer increase of 13.7% for cell line two. The bolus addition did not result in a changed process performance for the viability or the titer of cell line 1. This result indicates the potential of the process optimization by using an average model for, e.g., HSD processes with regard to metabolic phases.

4.4. Metabolic Flux Analysis of the HSD Process Supplemented with LAC/CYS

The breakpoints between the metabolic phases were identified with segmented linear modeling using the extracellular fluxes of the cell. In the next step, intracellular fluxes obtained by metabolic flux analyses were integrated into segmented modeling. Therefore, an MFA is performed for the HSD process supplemented with LAC/CYS.

We performed the MFA with a model from the literature [23] and with the MATLAB-based toolbox PFA [22]. The raw data of both processes were used to calculate the intracellular flux distribution for every day of the process. The MFA results for each day are shown for both processes in the heatmap as means in Figure 10. The fluxes are expressed in percent (normalized) as a function of process time (d). The highest uptake of glucose and flux through glycolysis can be seen in the beginning of the process, which then declines until day six, when lactate consumption is the highest. The low flux in the glycolysis is then compensated by uptake of lactate. From day eight onwards, the glycolytic flux increases again. At the end of the process, lactate is mostly not being metabolized anymore as the flux is around zero after day nine. Part of the flux flow in glycolysis goes from glucose-6-phosphate (G6P) into ribulose-5-phosphate (R5P) and subsequently into the pentose phosphate pathway (PPP). The flux into the PPP is low compared to the fluxes in other pathways. The flux into the PPP is the highest in the beginning and then decreases over time.

Besides the flux to lactate and to the PPP, the glucose flux goes into another major metabolic pathway. This pathway starts with the conversion of pyruvate into acetyl-CoA, which then enters the TCA cycle. Upon analyzing the flux map, the fluxes in the TCA cycle do not have high variations. The fluxes are mostly in a similar range with a minimum at day seven. Comparing the fluxes of TCA with glycolysis shows a higher flux in TCA than in glycolysis from day three onwards in the stationary phase [21,36]. This is due to the replenishment of the TCA by lactate. However, amino acids are also major contributors to the high fluxes in the TCA cycle. The same behavior could be observed in the MFA results of CHO cells performed with the same model [23,24] and in MFA results performed with other models [5,21,25,38–40].

4.5. Extended Segmented Modeling by Integration of Intracellular Fluxes

Intracellular fluxes obtained by MFA were integrated into segmented modeling. Integration of intracellular fluxes could lead to the identification of more phases that were not detected by only using extracellular fluxes. Furthermore, a metabolic flux analysis could give more insights into the shift in metabolic behavior which results in several metabolic phases. Therefore, the MFA results from the HSD10M + LAC/CYS data were integrated into segmented modeling together with the extracellular rates. The breakpoints of the metabolic shifts without intracellular fluxes for the HSD + LAC/CYS process were −0.046 1/d and 0.0147 1/d. The breakpoints with integration of the intracellular fluxes were −0.042 1/d and 0.0141 1/d. The breakpoints with both methods only differ in the

third decimal place. The identified breakpoints are therefore similar with and without integration of intracellular fluxes. This proves that segmented modeling only with extracellular rates is still a powerful tool for analyzing cell behavior in a fed-batch cell culture process.
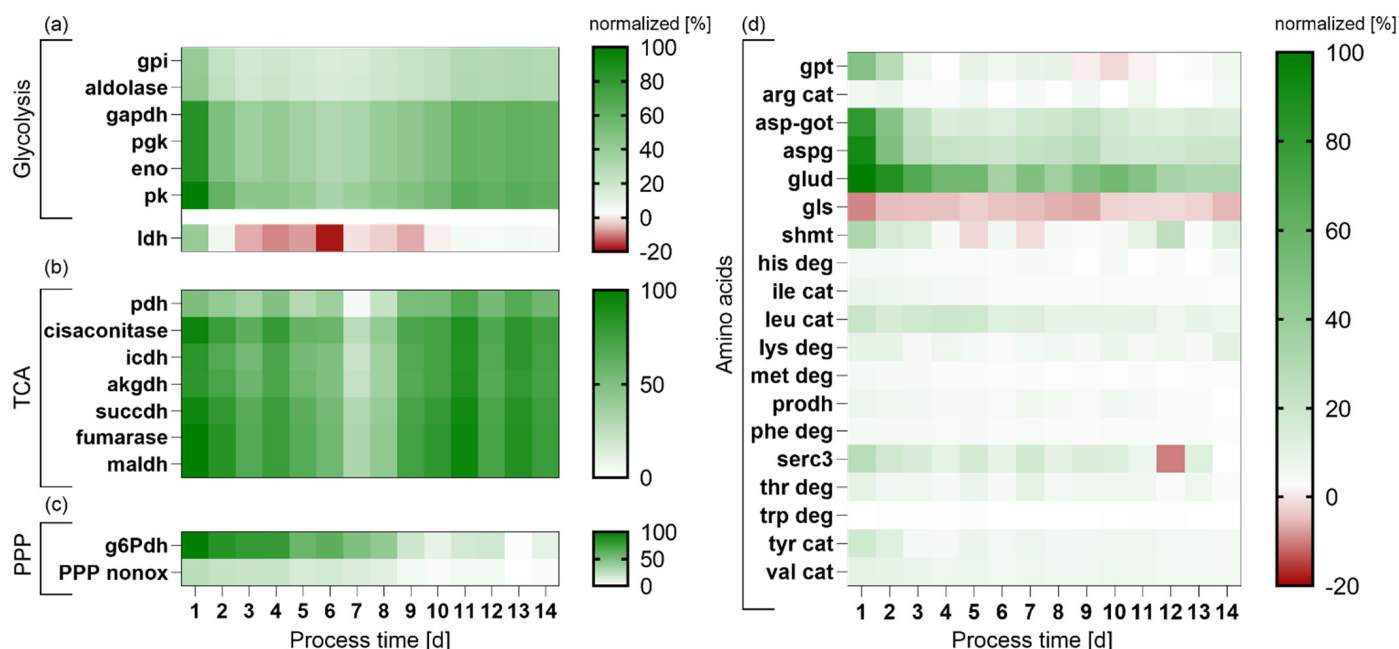

Figure 10. Heatmap of the metabolic flux analysis performed with the data of two identical uHSD10M + LAC/CYS processes. The fluxes are normalized in percent and are shown against the process time in days. The left side shows the intracellular fluxes which are part of the glycolysis and ldh (**a**), TCA cycle (**b**) and pentose phosphate pathway (PPP) (**c**), and the right side shows the amino acid metabolism (**d**). Glycolysis: gpi = glucosephosphateisomerase; gapdh = glyceraldehyde-3-phosphate dehydrogenase; pgk = phosphoglycerate kinase; eno = enolase; pk = pyruvate kinase; ldh = lactate dehydrogenase; TCA: pdh = pyruvate dehydrogenase; icdh = isocitrate dehydrogenase; akgdh = a-ketoglutarate dehydrogenase; succdh = succinyl-CoA synthetase; maldh = malate dehydrogenase; PPP: g6Pd = glucose-6-phosphate dehydrogenase; PPP nonox = pentose phosphate pathway non-oxidative part. Amino acids: gpt = glutamate-pyruvate transaminase; arg = arginine, asp-got = aspartate aminotransferase; aspg = aspartate transaminase; glud = glutamate dehydrogenase; gls = glutaminase; shmt = serine hydroxy methyltransferase; his = histidine; ile = isoleucine; leu = leucine; lys = lysine; met = methionine; prodh = proline dehydrogenase; phe = phenylalanine; serc3 = serine incorporator 3; thr = threonine; trp = tryptophan; tyr = tyrosine; val = valine; cat = catabolism; deg = degradation.

An MFA provided a deeper insight into the mechanism of the metabolic shift. The first phase is characterized by high fluxes through the glycolysis; these are divided into production of lactate and alanine and a high flux into the TCA. Further on, high fluxes of amino acids are used to replenish the TCA cycle. In the second phase, reduced fluxes occur in glycolysis, TCA and from most of the amino acids into TCA. To compensate for the low fluxes into the TCA, lactate is consumed instead of being produced. In the third phase, the flux in glycolysis and TCA increases again. Due to the higher uptake of glucose, lactate is consumed only at low levels. The metabolism of the amino acids in this phase is at the lowest level.

The redox metabolism—which was not part of the metabolic model—is probably a major reason for the metabolic shifts because the redox ratio is an important control variable. The redox effect, for example, the ratio of NADH to NAD+, can have powerful effects on many reaction rates [5]. The supply of NADH from the cytosol remains sufficient

until the glucose rate decreases. When the NADH supply becomes inadequate, the lactate concentration is high. This concentration, combined with a low redox, leads to the reversal in LDH. Therefore, lactate is consumed and NADH is produced. The redox variable increases more at the end of the process at high seeding densities with a higher feed compared to lower seeding densities [5]. This could explain why lactate consumption is reduced to zero as NADH is available in sufficient amounts due to glycolysis.

5. Conclusions and Outlook

The objectives of this study were defined into three areas. The first objective was the analysis and comparison of metabolic phases in conventional and high seeding density processes using segmented modeling. The methodology for segmented modeling was applied to identify the metabolic phases and to compare the trends in the central carbon metabolism. Segmented modelling improves our understanding of the metabolism of the HSD processes in comparison to standard process. The identified phases were similar for all HSD processes. The first phase is three days shorter in the HSD process compared to the STD process. Consequently, the third phase is increased by three days when the seeding density is increased compared to the STD process. However, the models generated with a specific rate of consumption or release of metabolites show similar trends in different phases, especially for glucose, lactate, ammonia, ASN and ALA. Therefore, the HSD process is not just shifted in time, but the metabolic phases are also changed. This contradicts studies that have concluded that the HSD process is only shifted in time [7]. As shown, the specific productivity and the overall titer thereby increase.

In the second objective, the segmented model was applied for feeding optimization in the HSD process using measured experiments. The insights provided by segmented modeling allowed further optimization of the process. The proposal based on the identified metabolic phases was to adjust the feed rate at the time point at which the metabolic shift occurs. This would meet the nutrient needs of the cells in the respective metabolic phase. The feeding regime adaption based on segmented modeling was implemented and exhibited an improved performance. A further proposal regarding feed optimization is to overcome the amino acid depletion in the first and second metabolic phases. A complementary study showed that optimizing the feeding strategy according to the metabolic phases led to two outcomes: (1) a reduction in the feeding amount without negative effects on process performance and (2) an increase in the titer for one cell line by overcoming amino acid depletion. This shows the potential of this approach of model-based optimization of feeding strategy considering metabolic phases.

In the third objective, a metabolic flux analysis was performed. The segmented model was extended by integration of intracellular fluxes. In the first part, the breakpoints between the metabolic phases were identified with segmented linear modeling using the extracellular fluxes of the cell. At the beginning it was assumed, that integration of intracellular phases from the MFA lead to the identification of more phases that were not detected when only using extracellular fluxes. Furthermore, this combines the segmented model with a constraint-based metabolic model. However, integration of the intracellular fluxes results in the identification of the same breakpoints and therefore the same phases. This strongly supports the previous identification of phases and proves the reliability of the calculations with extracellular phases. This proves that segmented modeling with extracellular rates is simple but effective; further integration of MFA results is not necessary for phase identification.

Looking ahead, segmented modeling has potential in subsequent modeling and prediction. Segmented modeling provides the basis for analyzing correlations between the different amino acids and their contribution to an increased productivity/viability. Overall, this work showed the potential of segmented modelling as a linear regression model representing the average characteristics of the cell phenotype. Further comprehensive analyses of amino acid composition in feed and basal media can facilitate designing experiments for the development and optimization of cell culture processes.

References

1. Tihanyi, B.; Nyitray, L. Recent Advances in CHO Cell Line Development for Recombinant Protein Production. *Drug. Discov. Today Technol.* **2020**, *38*, 25–34. [CrossRef] [PubMed]
2. Ritacco, F.V.; Wu, Y.; Khetan, A. Cell Culture Media for Recombinant Protein Expression in Chinese Hamster Ovary (CHO) Cells: History, Key Components, and Optimization Strategies. *Biotechnol. Progr.* **2018**, *34*, 1407–1426. [CrossRef] [PubMed]
3. Xu, W.-J.; Lin, Y.; Mi, C.-L.; Pang, J.-Y.; Wang, T.-Y. Progress in Fed-Batch Culture for Recombinant Protein Production in CHO Cells. *Appl. Microbiol. Biotechnol.* **2023**, *107*, 1063–1075. [CrossRef] [PubMed]
4. Fischer, S.; Marquart, K.F.; Pieper, L.A.; Fieder, J.; Gamer, M.; Gorr, I.; Schulz, P.; Bradl, H. MiRNA Engineering of CHO Cells Facilitates Production of Difficult-to-express Proteins and Increases Success in Cell Line Development. *Biotechnol. Bioeng.* **2017**, *114*, 1495–1510. [CrossRef]
5. Brunner, M.; Kolb, K.; Keitel, A.; Stiefel, F.; Wucherpfennig, T.; Bechmann, J.; Unsoeld, A.; Schaub, J. Application of Metabolic Modeling for Targeted Optimization of High Seeding Density Processes. *Biotechnol. Bioeng.* **2021**, *118*, 1793–1804. [CrossRef]
6. Ahn, W.S.; Antoniewicz, M.R. Towards Dynamic Metabolic Flux Analysis in CHO Cell Cultures. *Biotechnol. J.* **2012**, *7*, 61–74. [CrossRef]
7. Yang, W.C.; Lu, J.; Kwiatkowski, C.; Yuan, H.; Kshirsagar, R.; Ryll, T.; Huang, Y. Perfusion Seed Cultures Improve Biopharmaceutical Fed-batch Production Capacity and Product Quality. *Biotechnol. Progr.* **2014**, *30*, 616–625. [CrossRef]
8. Gong, X.; Li, D.; Li, X.; Fang, Q.; Han, X.; Wu, Y.; Yang, S.; Shen, B.Q. Fed-Batch Culture Optimization of a Growth-Associated Hybridoma Cell Line in Chemically Defined Protein-Free Media. *Cytotechnology* **2006**, *52*, 25–38. [CrossRef]
9. Stadermann, A.; Gamer, M.; Fieder, J.; Lindner, B.; Fehrmann, S.; Schmidt, M.; Schulz, P.; Gorr, I.H. Structural Analysis of Random Transgene Integration in CHO Manufacturing Cell Lines by Targeted Sequencing. *Biotechnol. Bioeng.* **2022**, *119*, 868–880. [CrossRef]
10. Brunner, M.; Bechmann, J.; Bollgoenn, E.; Unsoeld, A. Mammalian Cell Culture Processes. Application WO-2021165302-A1, 26 August 2021.
11. Prade, E.; Zeck, A.; Stiefel, F.; Unsoeld, A.; Mentrup, D.; Gutierrez, E.A.; Gorr, I.H. Cysteine in Cell Culture Media Induces Acidic IgG1 Species by Disrupting the Disulfide Bond Network. *Biotechnol. Bioeng.* **2021**, *118*, 1091–1104. [CrossRef]
12. Wang, J.; Zhou, L.; Lei, H.; Hao, F.; Liu, X.; Wang, Y.; Tang, H. Simultaneous Quantification of Amino Metabolites in Multiple Metabolic Pathways Using Ultra-High Performance Liquid Chromatography with Tandem-Mass Spectrometry. *Sci. Rep.* **2017**, *7*, 1423. [CrossRef] [PubMed]
13. Provost, A.; Bastin, G.; Agathos, S.N.; Schneider, Y.-J. Metabolic Design of Macroscopic Bioreaction Models: Application to Chinese Hamster Ovary Cells. *Bioproc. Biosyst. Eng.* **2006**, *29*, 349–366. [CrossRef] [PubMed]
14. Yahia, B.B.; Gourevitch, B.; Malphettes, L.; Heinzle, E. Segmented Linear Modeling of CHO Fed-batch Culture and Its Application to Large Scale Production. *Biotechnol. Bioeng.* **2017**, *114*, 785–797. [CrossRef] [PubMed]
15. Deshpande, R.; Yang, T.H.; Heinzle, E. Towards a Metabolic and Isotopic Steady State in CHO Batch Cultures for Reliable Isotope-based Metabolic Profiling. *Biotechnol. J.* **2009**, *4*, 247–263. [CrossRef]
16. Pirt, S.J. Maintenance Energy: A General Model for Energy-Limited and Energy-Sufficient Growth. *Arch. Microbiol.* **1982**, *133*, 300–302. [CrossRef]
17. Luedeking, R.; Piret, E.L. A Kinetic Study of the Lactic Acid Fermentation. Batch Process at Controlled PH. *J. Biochem. Microbiol.* **1959**, *1*, 393–412. [CrossRef]
18. Motulsky, H.J.; Brown, R.E. Detecting Outliers When Fitting Data with Nonlinear Regression—A New Method Based on Robust Nonlinear Regression and the False Discovery Rate. *BMC Bioinform.* **2006**, *7*, 123. [CrossRef]
19. Murtagh, F. A Survey of Recent Advances in Hierarchical Clustering Algorithms. *Comput. J.* **1983**, *26*, 354–359. [CrossRef]
20. Malash, G.F.; El-Khaiary, M.I. Piecewise Linear Regression: A Statistical Method for the Analysis of Experimental Adsorption Data by the Intraparticle-Diffusion Models. *Chem. Eng. J.* **2010**, *163*, 256–263. [CrossRef]
21. Nolan, R.P.; Lee, K. Dynamic Model for CHO Cell Engineering. *J. Biotechnol.* **2012**, *158*, 24–33. [CrossRef]
22. Morales, Y.; Bosque, G.; Vehí, J.; Picó, J.; Llaneras, F. PFA Toolbox: A MATLAB Tool for Metabolic Flux Analysis. *BMC Syst. Biol.* **2016**, *10*, 46. [CrossRef] [PubMed]

23. Brunner, M.; Doppler, P.; Klein, T.; Herwig, C.; Fricke, J. Elevated PCO2 Affects the Lactate Metabolic Shift in CHO Cell Culture Processes. *Eng. Life Sci.* **2018**, *18*, 204–214. [CrossRef]
24. Wahrheit, J.; Nicolae, A.; Heinzle, E. Dynamics of Growth and Metabolism Controlled by Glutamine Availability in Chinese Hamster Ovary Cells. *Appl. Microbiol. Biot.* **2014**, *98*, 1771–1783. [CrossRef]
25. Xing, Z.; Kenty, B.; Koyrakh, I.; Borys, M.; Pan, S.-H.; Li, Z.J. Optimizing Amino Acid Composition of CHO Cell Culture Media for a Fusion Protein Production. *Process Biochem.* **2011**, *46*, 1423–1429. [CrossRef]
26. Padawer, I.; Ling, W.L.W.; Bai, Y. Case Study: An Accelerated 8-day Monoclonal Antibody Production Process Based on High Seeding Densities. *Biotechnol. Progr.* **2013**, *29*, 829–832. [CrossRef] [PubMed]
27. Li, B.; Ryan, P.W.; Ray, B.H.; Leister, K.J.; Sirimuthu, N.M.S.; Ryder, A.G. Rapid Characterization and Quality Control of Complex Cell Culture Media Solutions Using Raman Spectroscopy and Chemometrics. *Biotechnol. Bioeng.* **2010**, *107*, 290–301. [CrossRef] [PubMed]
28. Ali, A.S.; Raju, R.; Kshirsagar, R.; Ivanov, A.R.; Gilbert, A.; Zang, L.; Karger, B.L. Multi-Omics Study on the Impact of Cysteine Feed Level on Cell Viability and MAb Production in a CHO Bioprocess. *Biotechnol. J.* **2019**, *14*, 1800352. [CrossRef] [PubMed]
29. Sengupta, N.; Rose, S.T.; Morgan, J.A. Metabolic Flux Analysis of CHO Cell Metabolism in the Late Non-growth Phase. *Biotechnol. Bioeng.* **2011**, *108*, 82–92. [CrossRef]
30. Stepper, L.; Filser, F.A.; Fischer, S.; Schaub, J.; Gorr, I.; Voges, R. Pre-Stage Perfusion and Ultra-High Seeding Cell Density in CHO Fed-Batch Culture: A Case Study for Process Intensification Guided by Systems Biotechnology. *Bioproc. Biosyst. Eng.* **2020**, *43*, 1431–1443. [CrossRef]
31. Zagari, F.; Jordan, M.; Stettler, M.; Broly, H.; Wurm, F.M. Lactate Metabolism Shift in CHO Cell Culture: The Role of Mitochondrial Oxidative Activity. *New Biotechnol.* **2013**, *30*, 238–245. [CrossRef]
32. Vodopivec, M.; Lah, L.; Narat, M.; Curk, T. Metabolomic Profiling of CHO Fed-batch Growth Phases at 10, 100, and 1000 L. *Biotechnol. Bioeng.* **2019**, *116*, 2720–2729. [CrossRef] [PubMed]
33. Traustason, B. Amino Acid Requirements of the Chinese Hamster Ovary Cell Metabolism during Recombinant Protein Production. *BioRxiv* **2019**. [CrossRef]
34. Lane, A.N.; Fan, T.W.-M. Regulation of Mammalian Nucleotide Metabolism and Biosynthesis. *Nucleic Acids Res.* **2015**, *43*, 2466–2485. [CrossRef] [PubMed]
35. Li, J.; Wong, C.L.; Vijayasankaran, N.; Hudson, T.; Amanullah, A. Feeding Lactate for CHO Cell Culture Processes: Impact on Culture Metabolism and Performance. *Biotechnol. Bioeng.* **2012**, *109*, 1173–1186. [CrossRef] [PubMed]
36. Coulet, M.; Kepp, O.; Kroemer, G.; Basmaciogullari, S. Metabolic Profiling of CHO Cells during the Production of Biotherapeutics. *Cells* **2022**, *11*, 1929. [CrossRef] [PubMed]
37. Mulukutla, B.C.; Kale, J.; Kalomeris, T.; Jacobs, M.; Hiller, G.W. Identification and Control of Novel Growth Inhibitors in Fed-batch Cultures of Chinese Hamster Ovary Cells. *Biotechnol. Bioeng.* **2017**, *114*, 1779–1790. [CrossRef]
38. Ahn, W.S.; Antoniewicz, M.R. Metabolic Flux Analysis of CHO Cells at Growth and Non-Growth Phases Using Isotopic Tracers and Mass Spectrometry. *Metab. Eng.* **2011**, *13*, 598–609. [CrossRef]
39. Goudar, C.; Biener, R.; Boisart, C.; Heidemann, R.; Piret, J.; de Graaf, A.; Konstantinov, K. Metabolic Flux Analysis of CHO Cells in Perfusion Culture by Metabolite Balancing and 2D [13C, 1H] COSY NMR Spectroscopy. *Metab. Eng.* **2010**, *12*, 138–149. [CrossRef]
40. Schaub, J.; Clemens, C.; Kaufmann, H.; Schulz, T.W. Genomics and Systems Biology of Mammalian Cell Culture. *Adv. Biochem. Eng. Biotechnol.* **2011**, *127*, 133–163. [CrossRef]